Spin Accumulation and Equilibrium Currents at the Edge of 2DEGs with Spin-Orbit Coupling

Gonzalo Usaj and C. A. Balseiro

Instituto Balseiro and Centro Atómico Bariloche, Comisión Nacional de Energía Atómica, (8400) San Carlos de Bariloche, Argentina.

Abstract. – We show that in a two dimensional electron gas (2DEG) the interplay between the Rashba spin-orbit coupling and a potential barrier (*eg.*, the sample edge) generates interesting spin effects. In the presence of an external charge current, a *spin accumulation* is built up near the barrier while in equilibrium there is an inhomogeneous spin current which is localized at the barrier and flows parallel to it. When an in-plane magnetic field perpendicular to the barrier is applied, the system also develops an inhomogeneous *charge current* density. These effects originate purely from the structure of the eigenstates near the boundary.

Spintronics has recently emerged as an active field of research due to its potential impact on both the design of future electronic devices and quantum computing [1]. The ultimate goal of spintronics is the manipulation and coherent control of the electronic spin degrees of freedom. This requires the ability to generate, inject and control spin-polarized currents in electronic devices—an example of that is the spin-transistor proposal by Datta and Das [2]. In recent years, the spin-orbit coupling has been recognized as an efficient tool to manipulate the electron's spin leading to a substantial amount of work devoted to study its effect on the transport properties of nanostructures and two dimensional electron gases (2DEG) [3–13]. An important step along this line was the recently reported observation of the predicted spin Hall effect (SHE) [14, 15]: when a transport current flows through the system the opposite spins accumulate at the lateral edges of the sample. It has been argued that the SHE can be an extrinsic effect when it relies on impurity scattering [16, 17] or an intrinsic effect when it originates from the spin-orbit coupling in a 2DEG [18, 19].

In this Letter we show that in a ballistic 2DEG with Rashba spin-orbit coupling [20, 21] the presence of a potential barrier in one direction leads to a *current induced spin accumulation* at the sample edge. The effect is reminiscent of the intrinsic SHE although in our case it is based purely on geometric properties of the clean systems. In addition, we show that there is an equilibrium spin current [22]—ie. with no external fields applied—that flows parallel to the barrier, and an *inhomogeneous charge current density* when an in-plane magnetic field is applied. These intrinsic effects are relevant for a better understanding of spin-sensitive transport experiments and numerical results in small systems [23–26].
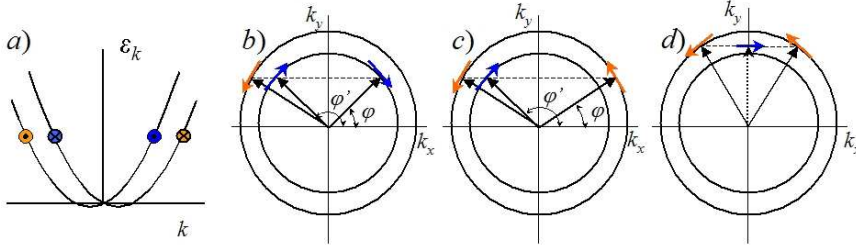
Fig. 1 – Schematics of the band structure. The dots show the spin orientation in the two bands. The others panels show all possible configurations (for $\varepsilon > 0$) of the incident plane wave and the corresponding spin orientation together with the two Fermi surfaces: b) incident plane wave in the '+' band; c) incident plane wave in the '−' band with $|k_y| < k_+$, and d) with $|k_y| > k_+$. In the latter case, the reflected component on the '+' band is an evanescent mode whose spin points out of the plane.

We consider a 2DEG with Rashba spin-orbit coupling. The Hamiltonian is then given by

$$ H = \frac{p_x^2 + p_y^2}{2m^*} + V(\boldsymbol{r}) + \frac{\alpha}{\hbar}\left(p_y \sigma_x - p_x \sigma_y\right) , \tag{1} $$

where $V(\boldsymbol{r})$ is the confining potential in the plane of the 2DEG, m^* is the effective mass and α is the Rashba coupling constant [6,27]. For a system with translational invariance ($V(\boldsymbol{r}) = 0$), the eigenfunctions of Hamiltonian (1) are given by

$$ \Psi_\pm(\boldsymbol{r}) = \frac{1}{\sqrt{2A}} e^{i\,\boldsymbol{k}\cdot\boldsymbol{r}} \begin{pmatrix} \pm e^{-i\phi/2} \\ e^{i\phi/2} \end{pmatrix} , \tag{2} $$

with $e^{i\phi} = (k_y - ik_x)/k$ and A the system's area. Notice that if we write $\boldsymbol{k} = k(\cos\varphi, \sin\varphi)$, then $\phi = \varphi - \pi/2$. Consequently, these modes have the spin in the plane of the 2DEG pointing in a direction perpendicular to the wavevector $\boldsymbol{k}$ as schematically shown in Fig. 1. The spin degeneracy is lifted by the spin-orbit coupling leading to two non-degenerated bands with the following dispersion relation: $\varepsilon_\pm(\boldsymbol{k}) = \hbar^2 k^2/2m^* \pm \alpha k$.

Let us now consider a system with a sharp edge in the x-direction defined by the potential $V(\boldsymbol{r}) \equiv V_0 \Theta(x)$ with $\Theta(x)$ the step-function. For $V_0 \gg E_{\mathrm{F}}$, where E_{F} is the Fermi energy, the boundary condition imposes the eigenfunctions with $\varepsilon_\pm \leq E_{\mathrm{F}}$ to be zero for $x \geq 0$ (the exponential tail inside the barrier is negligible). For $x \leq 0$ they can be written as superposition of incident and reflected waves and for positive energy ε we have:

$$ \Psi_{\boldsymbol{k},s}(\boldsymbol{r}) = \frac{e^{i\,k_y y}}{C^{\frac{1}{2}}} \left\{ e^{i\,k_x x} \begin{pmatrix} s e^{-i\phi/2} \\ e^{i\phi/2} \end{pmatrix} + R\, e^{-i\,k_x x} \begin{pmatrix} s e^{i\phi/2} \\ e^{-i\phi/2} \end{pmatrix} + R'\, e^{-i\,k_x' x} \begin{pmatrix} -s e^{-i\phi'/2} \\ e^{i\phi'/2} \end{pmatrix} \right\} , \tag{3} $$

where $s = \pm 1$ is the band index of the incident plane wave with wavevector (k_x, k_y), C is a normalization constant, $(-k_x, k_y)$ and $(-k_x', k_y) = k_{-s}(\cos\varphi', \sin\varphi')$ are the wavevectors of the reflected plane waves, $k_s = [(2\hbar^2\varepsilon/m^* + \alpha^2)^{\frac{1}{2}} - s\alpha]m^*/\hbar^2$ and

$$ R = -\frac{\cos([\varphi - \varphi']/2)}{\sin([\varphi + \varphi']/2)}, \quad R' = \frac{i\cos\varphi}{\sin([\varphi + \varphi']/2)} . $$

For $\varphi \neq 0$, the reflected wave has a non-zero amplitude in both bands as illustrated in Fig.1 (this is a simple way to create polarized beams out of an unpolarized one [28, 29]). When the

incident plane wave is on the $s = -1$ band, the above solution remains valid only if $|k_y| \leq k_+$ For $|k_y| > k_+$ there are no propagating modes in the "+" band and evanescent modes localized at the boundary appear (Fig.1d). In that case k_x' is replaced by an imaginary wavevector and the corresponding spinor acquires an explicit projection on the z axis:

$$\Psi_{\boldsymbol{k},-}(\boldsymbol{r}) = \frac{e^{i\,k_y y}}{C'^{\frac{1}{2}}} \left\{ e^{i\,k_x x} \begin{pmatrix} -e^{-i\phi/2} \\ e^{i\phi/2} \end{pmatrix} + e^{i\,\Theta}\, e^{-i\,k_x x} \begin{pmatrix} -e^{i\phi/2} \\ e^{-i\phi/2} \end{pmatrix} + R_{ev}\, e^{Kx} \begin{pmatrix} a \\ b \end{pmatrix} \right\}, \qquad (4)$$

with $K = (k_y^2 - k_+^2)^{\frac{1}{2}}$ and $a^2/b^2 = (k_y + K)/(k_y - K)$. Since the incident and the reflected plane waves have different spin projections, their interference leads to a non-zero spin density on the z-axis, $\langle \hat{\sigma}_z \rangle_{\boldsymbol{k},s} = \Psi_{\boldsymbol{k},s}^{\dagger}(\boldsymbol{r}) \hat{\sigma}_z \Psi_{\boldsymbol{k},s}(\boldsymbol{r})$ with some spin accumulation at the sample edge ($x \lesssim 0$). The sign of the spin accumulation depends on the sign of the conserved component k_y of the wavevector. Consequently, in the ground state where states with positive and negative values of k_y are occupied, the contribution to the local magnetization of each band is zero. However, if there were a preferential motion of the carriers in the y-direction—imposed by an external current, for instance—there would be a net magnetization at the surface. To illustrate this effect, we consider an ideal ballistic system where the voltage drops at the contacts and the electric field is zero at the interior of the sample. Then, in the energy interval $[E_F + eV/2, E_F - eV/2]$, only states with $k_y \geq 0$ are occupied within the sample [30] and we obtain (for $E_F > eV/2$):

$$\langle \hat{\sigma}_z(x) \rangle = \sum_{\boldsymbol{k},s;k_y > 0} \langle \hat{\sigma}_z \rangle_{\boldsymbol{k},s}\, F_{\boldsymbol{k},s}(E_F, eV) \qquad (5)$$

with $F_{\boldsymbol{k},s}(E_F, eV) = \Theta(E_F + eV/2 - \varepsilon_s(\boldsymbol{k})) - \Theta(E_F - eV/2 - \varepsilon_s(\boldsymbol{k}))$ [31]. For small eV only states at E_F contribute to the sum and we may separate the contribution of the states with evanescent waves (Eq. (4)) from the rest (Eq. (3)). For any E_F, the former contribution can be scaled onto the $E_F = 0$ result (shown in Fig.2a) when plotted as a function of $(k_-^2 - k_+^2)^{\frac{1}{2}} x$. From this scaling law, it can be shown that the integrated spin accumulation due to this contribution decreases with E_F as $(E_F + \alpha^2 m^*/2\hbar^2)^{-\frac{3}{4}}$. As we show below, states with reflected waves in the two bands (Eq. (3)) tend to cancel the effect, leading to a faster decay of the spin accumulation as a function of E_F. While the eigenfunctions presented above give a clear physical picture of the edge effect, an analytical calculation is not simple since: a) the two modes of Eq. (3) are not orthogonal to each other; b) a proper counting of modes requires to work with a system of finite width L_x. In what follows we present results obtained by a numerical integration of the Schrödinger equation using finite differences. One advantage of the method is that it is not restricted to a square well confining potential—our results hold in the case of a sharp parabolic potential—and is equivalent to use a tight- binding version of Hamiltonian (1) [32],

$$\begin{aligned} H = & \sum_{n\sigma} \varepsilon_\sigma c_{n\sigma}^{\dagger} c_{n\sigma} - \sum_{<n,m>\sigma} t_{nm} c_{n\sigma}^{\dagger} c_{m\sigma} + h.c. \\ & - \lambda \sum_{n} \left\{ i \left(c_{n\uparrow}^{\dagger} c_{(n+\hat{y})\downarrow} + c_{n\downarrow}^{\dagger} c_{(n+\hat{y})\uparrow} \right) - \left(c_{n\uparrow}^{\dagger} c_{(n+\hat{x})\downarrow} - c_{n\downarrow}^{\dagger} c_{(n+\hat{x})\uparrow} \right) \right\} + h.c. \qquad (6) \end{aligned}$$

here $c_{n\sigma}^{\dagger}$ creates an electron at site n with spin $\sigma_z = \sigma$ and energy $\varepsilon_\sigma = 4t$, $t = \hbar^2/2m^* a_0^2$, $a_0 = 5$nm is the lattice parameter, and $\lambda = \alpha/2a_0$. The summation is carried out on a square lattice where the coordinate of site n is $\boldsymbol{r}_n = n_x \hat{x} + n_y \hat{y}$ with $\hat{x}$ and $\hat{y}$ the unit lattice vectors. The hopping matrix element $t_{nm} = t$ connects nearest neighbors. All quantities presented
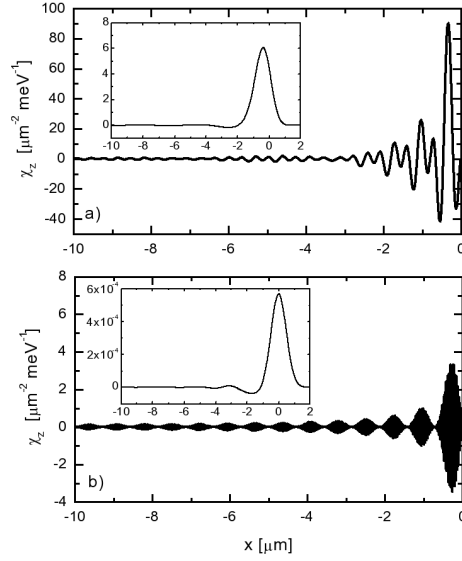
Fig. 2 – Current-induced spin accumulation, $\chi_z(x, E_F)$, close to the potential barrier (edge) for $E_F = 0$ (a) and $E_F = 5$meV (b). The insets show the convolution with a Gaussian with an rms of 0.5μm.

below are obtained from the one particle propagators (for details see Ref. [11]). We first present results for systems with a large width L_x and then we discuss the effect of the lateral confinement in a quantum wire of reduced L_x.

To analyze the spin accumulation we linearize Eq. (5) and define $\chi_z(x) = \langle\hat{\sigma}_z(x)\rangle/eV$. The total spin accumulation for $E_F = 0$ is shown in Fig.2a. The inset shows the convolution with a Gaussian with an rms. of $0.5\,\mu$m. For $E_F > 0$ ($k_+ \neq 0$), the contribution from the states with $|k_y| < k_+$ partially cancels the effect as shown in Fig. 2b. Thus, the maximum spin accumulation is obtained at $E_F = 0$ and as the carrier density increases it decreases and tends to zero. $\chi_z(x)$ is strongly dependent on E_F so even for moderate values of eV, non-linear effects are observed and Eq. (5) should be used.

In this ballistic regime, the charge current also generates a local magnetization $\langle\hat{\sigma}_x(x)\rangle$ in the x-direction (*i.e.* in the plane of the 2DEG and perpendicular to the sample edge) [24] while by symmetry $\langle\hat{\sigma}_y(x)\rangle \equiv 0$ [4]—the non-zero value obtained for finite systems [24] is a consequence of the reflections at the sample-lead interfaces and depends strongly on the characteristics of such interface [33]. *It is important to emphasize that the spin accumulation at the edge is a purely geometric effect.* It is not directly connected to the one discussed in Ref. [18]. The latter is due to an electric field induced spin current, which is absent in the ballistic regime studied here.

Another consequence of the symmetry of $\langle\hat{\sigma}_z\rangle_{k,s}$ with respect to k_y is the presence of spin currents along the edges of the sample. In equilibrium, we define the spin current density as:

$$J_y^{\sigma_z}(x) = \frac{\hbar}{4} \sum_{\text{occ}} \langle\hat{v}_y\hat{\sigma}_z + \hat{\sigma}_z\hat{v}_y\rangle_{k_y,\nu} = \frac{\hbar^2}{2m^*} \sum_{\text{occ}} k_y\langle\hat{\sigma}_z\rangle_{k_y,\nu} \qquad (7)$$

here $\hat{v}_y = \mathrm{i}/\hbar[\hat{H}, \hat{y}] = \hat{p}_y/m^* + \alpha\hat{\sigma}_x/\hbar$ is the y-component of the velocity operator and the summation is restricted to all occupied states with quantum numbers k_y and ν. Here again the evanescent modes play a central role and $J_y^{\sigma_z}(x)$ is *non-zero* in equilibrium. Figs. 3a
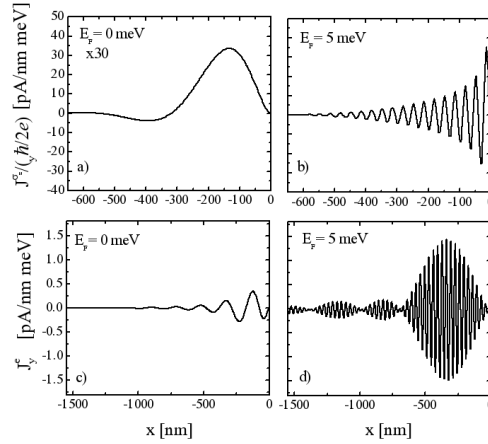
Fig. 3 – Total spin (a,b) and charge (c,d) current density in the vicinity of the edge for different values of E_F. Notice the currents are localized near the edge. Here $g\mu_B B_x = 0.25$meV and $\alpha = 5$meVnm.

and 3b show the total spin current density $J_y^{\sigma_z}(x)$ for different values of E_F. The total spin current oscillates with a characteristic wavevector $k_{F,+} + k_{F,-}$ and decays toward the bulk of the sample with a characteristic length $(k_{F,-} - k_{F,+})^{-1} = \hbar^2/2m^*\alpha \approx 100$nm that is energy independent. This longitudinal spin current, integrated in half of the sample— from $-L_x/2$ to 0— is non-zero: spin flows in opposite directions on opposite sides of the sample. It is worth pointing out that this current does not violates time reversal symmetry [22].

The counterpart of the current induced magnetization at the sample edge, is the generation of edge currents by a magnetic field. To avoid the diamagnetic coupling and Landau quantization, we now analyze the response of the system to an external in-plane magnetic field. In the continuous model, the propagating modes are still given by Eq. (3) but the spinor's angle is such that $e^{i\phi} = z/|z|$ with $z = \alpha(k_y - ik_x) + \frac{1}{2}g\mu_B(-B_x + iB_y)$ and g the g-factor. The presence of the magnetic field modifies the Fermi surface which is now given by $E_F = \hbar^2 k^2/2m^* \pm |z|$. Notice it is not longer a circle. It is then clear that the magnetic field introduces an asymmetry between k_y and $-k_y$ when applied in the x-direction. In bulk, the charge current induced by the field is zero due to a cancellation between the contributions of the two bands. However, at the edge the evanescent modes lead to the appearance of a non-zero *charge current density*,

$$J_y^e(x, \varepsilon) = e \sum_{k_y, \nu} \langle v_y \rangle_{k_y, \nu}\, \delta(\varepsilon - \varepsilon_{k_y, \nu}) \tag{8}$$

The total current density, $J_y^e(x)$, is obtained by integration of this quantity up to E_F. Figs. 3c and 3d shows $J_y^e(x)$ for $E_F = 0$ and 5meV. As in the case of the spin current, the charge current is localized at the surface and presents modulations with two characteristic wavelengths, $\lambda_F/2 = 2\pi/(k_{F,+} + k_{F,-})$ and $\lambda_\alpha = 2\pi/(k_{F,-} - k_{F,+})$.

So far we have presented results for wide (large L_x) systems. We have shown that out of equilibrium, when a ballistic transport current flows in the system, there is spin accumulation at the edges. The spin and charge current densities discussed above are properties of the ground state and depend on a delicate balance of the contribution of states with and without evanescent waves. At a given energy, the number of states of each type can be changed by engineering the sample geometry and thus altering the partial cancellation. In particular this
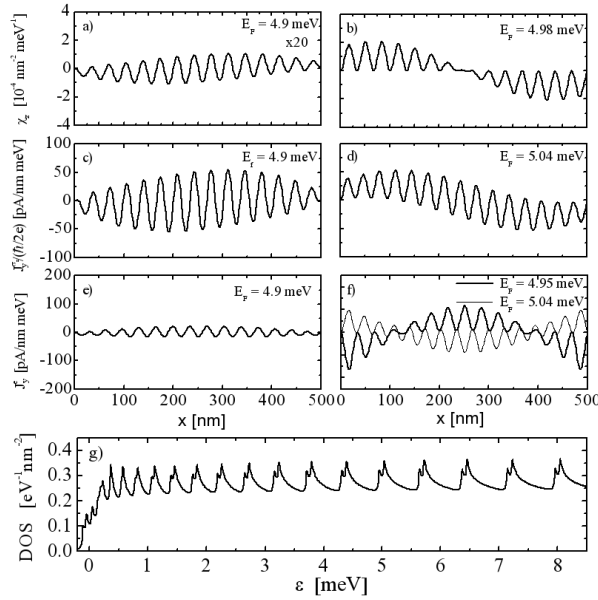
Fig. 4 – Current-induced spin accumulation (a, b) in the absence of a magnetic field and charge (c, d) and spin (e,f) current density in the presence of an in-plane magnetic field for a quantum wire. The panels on the left (a, c and d) correspond to the case of a non-resonant energy, $\varepsilon = 4.9$meV, while the panels on the right (b, d and e) correspond to resonant cases, $\varepsilon = 4.98$meV, $\varepsilon = 4.95$meV and 5.04meV respectively. We used: $g\mu_B B_x = 0.25$meV, $L = 500$nm and $\alpha = 5$meVnm. Panel (g) shows the density of states in the presence of the magnetic field. Notice the singularities are split.

can be done in a narrow (small L_x) quantum wire. The lateral confinement of the 2DEG in the x-direction leads to the quantization of the transverse modes and the density of states presents quasi-one dimensional van Hove singularities (see Fig. 4g). When E_F is tuned to be close to a singularity, there are many states with $k_y \sim 0$—thus with no evanescent waves—that define the behavior of the system.

The results for the current-induced spin accumulation, obtained using the tight-binding approach, are shown in Figs. 4a and 4b in the absence of a magnetic field. Since the wavefunctions of the states with $k_y = 0$ have a simple form $\Psi_\pm(x) = L_x^{-\frac{1}{2}} \exp(\mp i\pi x/\lambda_\alpha) \sin(n\pi x/L_x) \left(\begin{smallmatrix} \pm i \\ 1 \end{smallmatrix}\right)$, where n is the channel index, one can readily show that, for $k_y \gtrsim 0$, $\langle\sigma_z\rangle \propto \sin^2(n\pi x/L_x) \sin(2\pi(x - L_x/2)/\lambda_\alpha))$ in excellent agreement with the numerical result of Fig. 4b ($n = 15$ for $E_F \approx 5$meV). In this case, the sign of the magnetization at the edges also depends on the ratio L_x/λ_α. For the parameters used in Fig. 4b the spin density is positive in the interval $[0, L_x/2]$. Figs. 4c and 4d shows the spin current profile. The resonant case presents well defined signs: there is a net spin current flowing in one direction on the right and in the opposite on the left.

The charge current density in the presence of an in-plane field is shown in Figs. 4e and 4f. For $|B_x| \ll 2\alpha k_F/g\mu_B$ a similar calculation as above gives $\langle v_y\rangle_\pm \propto \pm \sin^2(n\pi x/L_x) \cos(2\pi(x - L_x/2)/\lambda_\alpha))$. Though this expression does not fit the numerical result exactly (Fig 4f), it contains the correct spatial modulations. In particular, it shows that the charge current density changes its sign in a length scale given by $\lambda_\alpha/2$. It is also straightforward to check that the van Hove singularity is split by the magnetic field—the energy splitting being $\Delta \approx g\mu_B B_x |\sin(\pi L_x/\lambda_\alpha)|\lambda_\alpha/L_x\pi$ for $n \gg L_x/\lambda_\alpha$ (see Fig. 4g).

In summary, we showed that the presence of a potential barrier in systems with spin-orbit coupling leads to the appearance of current-induced magnetization at the sample edges and of equilibrium spin and charge current densities. These effects are important for a correct interpretation of numerical results in finite systems, where geometry plays a crucial role. On the experimental side, low density ballistic 2DEGs or quantum wires are required in order to observe the spin accumulation described here. It is worth mentioning, that these conditions are not met by the recent experiment of Ref. [34], where disorder is very large.

$$* * *$$

REFERENCES

[1]   Awschalom D., Samarth N. and Loss, D., *Semiconductor Spintronics and Quantum Computation* (Springer, New York) 2002
[2]   Datta S. and Das B., *Appl. Phys. Lett.*, **56** (1990) 665
[3]   Moroz A. V. and Barnes C. H. W., *Phys. Rev. B*, **60** (1999) 14272
[4]   Governale M. and Zülicke U., *Phys. Rev. B*, **66** (2002) 073311
[5]   Bellucci S. and Onorato P., *Phys. Rev. B*, **68** (2003) 245322
[6]   Miller J. B. *et al.*, *Phys. Rev. Lett.*, **90** (2003) 076807
[7]   Streda P. and Seba P., *Phys. Rev. Lett.*, **90** (2003) 256601
[8]   Mishchenko E. G. and Halperin B. I., *Phys. Rev. B*, **68** (2003) 045317
[9]   Schliemann J. and Loss D., *Phys. Rev. B*, **68** (2003) 165311
[10] Egues J. C., Burkard G. and Loss D., *App. Phys. Lett.*, **82** (2003) 2658
[11] Usaj G. and Balseiro C. A., *Phys. Rev. B*, **70** (2004) 041301(R)
[12] Rokhinson L. P. *et al.*, *Phys. Rev. Lett.*, **93** (2004) 146601
[13] Mishchenko E. G., Shytov A. V. and Halperin B. I., *Phys. Rev. Lett.*, **93** (2004) 226602
[14] Kato Y. K., Myers R. C., Gossard A. C. and Awshalom D. D., *Science*, **306** (2004) 1910
[15] Wunderlich J., Kaestner B., Sinova J. and Jungwirth T., *Phys. Rev. Lett.*, **94** (2005) 047204
[16] Dyakonov M. I. and Perel V. I., *JETP Lett.*, **13** (1971) 467; *Phys. Lett. A*, **35** (1971) 459
[17] Hirsch J. E., *Phys. Rev. Lett.*, **83** (1999) 1834
[18] Sinova J. *et al.*, *Phys. Rev. Lett.*, **92** (2004) 126603
[19] Murakami S., Nagaosa N. and Zhang S. C., *Science*, **301** (2003) 1348
[20] Rashba E. I., *Sov. Phys. Solid State*, **2** (1960) 1109
[21] Bychkov Y. A. and Rashba E. I., *JETP Lett.*, **39** (1984) 78
[22] Rashba E. I., *Phys. Rev. B*, **68** (2003) 241315(R)
[23] Sheng L., Sheng D. N. and Ting C. S., *Phys. Rev. Lett.*, **94** (2005) 016602
[24] Nikolic B. K., Souma S., Zarbo L. P. and Sinova J., *Phys. Rev. Lett.*, **95** (2005) 046601
[25] Nikolic B. K., Zarbo L. P. and Souma S., cond-mat/0408693
[26] Hankiewicz E. M., Molenkamp L., Jungwirth T. and Sinova J., cond-mat/0409334
[27] Nitta J., Akazaki T., Takayanagi H. and Enoki T., *Phys. Rev. Lett.*, **78** (1997) 1335
[28] Khodas M., Shekhter A. and Finkel'stein A. M., *Phys. Rev. Lett.*, **92** (2004) 086602
[29] Chen H. *et al.*, *Appl. Phys. Lett.*, **86** (2005) 032113
[30] Datta S., *Electronic transport in mesoscopic systems* (Cambridge Univ. Press) 1995
[31] Note that $\langle\ldots\rangle_{k,s}$ has to be calculated with the orthogonalized states, see below.
[32] Ando T., *Phys. Rev. B*, **40** (1989) 5325
[33] Reynoso A., Usaj G. and Balseiro, C. A., cond-mat/0511750
[34] Sih V. *et al.*, cond-mat/0506704